Nanoscale

Accepted Manuscript

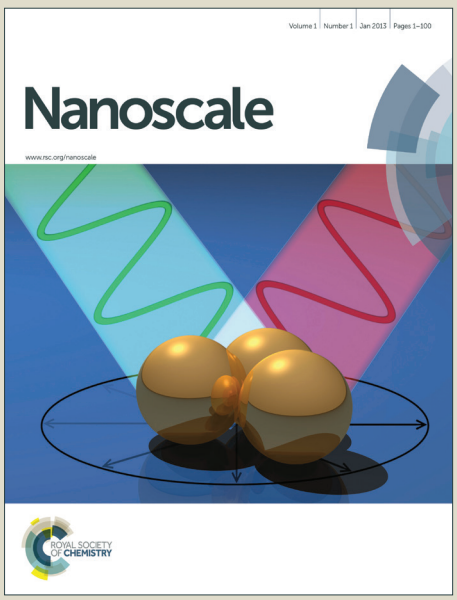

ROYAL SOCIETY OF CHEMISTRY

www.rsc.org/nanoscale

	Chinese Academy of Sciences, State Key Laboratory of Luminescence and Applications Zhao, Huiying; University of Jilin, Department of Basic Medicine, Gerontology Department of First Bethune Hospital Zhang, Hong; University of Amsterdam, Molecular Photonics - vant Hoff Institute for Molecular Sciences (HIMS)

Cite this: DOI: 10.1039/c0xx00000x

www.rsc.org/xxxxxx

ARTICLE TYPE

Towards high quality triangular silver nanoprisms: improved synthesis, six-tip based hot spots and ultra-high local surface plasmon resonance sensitivity

Bin Xue,[a,b,+] Dan Wang,[a,b,+] Jing Zuo,[a,b] Xianggui Kong,*[a] Youlin Zhang,[a] Xiaomin Liu,[a] Langping Tu,[a,b] Yulei Chang,[a] Cuixia Li,[a,b] Fei Wu,[a,b] Qinghui Zeng,[a] Haifeng Zhao,[a] Huiying Zhao[c] and Hong Zhang*[a, d]

Received (in XXX, XXX) Xth XXXXXXXXX 20XX, Accepted Xth XXXXXXXXX 20XX

DOI: 10.1039/b000000x

Abstract

The great application potential of triangular silver nanoprisms (TSNPRs, also referred to as triangular silver nanoplates) is hampered by lack of method in producing well-defined tips with high monodispersity, and easily removed ligands. In this work, simple one-step plasmon-mediated method was developed to prepare monodispersed triangular TSNPRs with high quality. In this approach, the sole surface capping agent was the easily removable trisodium citrate. Different from common strategy using complex polymers, OH^- ions were used to improve the monodispersity of silver seeds, as well as to control the growth process through inhibiting the oxidation of silver nanoparticles. Using these monodispersed high quality TSNPRs as building blocks, self-assembled TSNPRs consisting of six-tip based "hot spots" were realized for the first time as demonstrated in a high enhancement (~10^7) of surface-enhanced Raman Scattering (SERS). From plasmon band shift versus refractive index, ultra-high local surface plasmon resonance sensitivity (413 nm RIU^{-1} or 1.24 eV RIU^{-1}, figure of merit (FOM) =4.59) was reached at ~630 nm, making these materials promising for chemical/biological sensing applications.

1. Introduction

Noble metal nanoparticles hold great promise for various applications due to their unique optical, electrical, and chemical properties.[1-3] Triangular silver nanoprisms (TSNPRs, also referred to as silver nanoplates) as a classical noble metal nanoparticle,[4, 5] have potential applications in solar cell, surface-enhanced Raman Scattering (SERS), catalysis, bio-applications.[6-11] These applications depend not only on the intense tunable plasmonic band of TSNPRs, but also heavily on the sharp tip morphology. On one hand, sharp tip morphology has huge electric field enhancement around the tips of nanoprisms.[12, 13] Recently, bowtie nanoantenna forming the "hot spots" which consists of two triangular nanoparticles facing tip to tip has been demonstrated to drastically amplify the electric field between the two tips.[14, 15] On the other hand, tips of TSNPRs are sensitive to the position of their local surface plasmon resonance (LSPR) peaks.[16, 17] Utilization of these sharp tips, TSNPRs exhibit ultra-high LSPR sensitivity for chemical/biological sensing, have been used for detecting DNA, aptamer, glucose, Hg^+ ions.[18-21] Therefore, high quality TSNPRs can not only generate giant electric field enhancement around their tips and form tip-based hot spots, but also fabricate various tip sensitive chemical/biological sensors. However, preparation of TSNPRs with well-defined tips is difficult, especially in a relatively simple method for practical applications.

TSNPRs were first synthesized by the pioneers of Jin, Mirkin and co-workers using plasmon-mediated method in 2001[22] and improved later.[23-25] Different strategies have also been developed divided mainly into plasmon-mediated[26-28] and ligand-assisted chemical reduction methods.[29-31] Though ligand-assisted chemical reduction methods are easier to follow, the resulting TSNPRs show wide size distribution and tips are often truncated to some extent. Moreover, in most synthesis, polymers are often added, which are difficult to remove in certain applications (*e.g.* catalysis, SERS).[32, 33] Plasmon-mediated method could produce uniform TSNPRs with well-defined triangular shape. However, the drawback of this method is that it usually involved complex procedures. Though there was attempt to simplify the plasmon-mediated method,[27] the resulting TSNPRs are not uniform and mostly truncated.

In this work, we have developed a simple one-step plasmon-mediated method to prepare well-defined TSNPRs. Apart from using the easily removable citrates as surface capping agents, we introduced OH^- ions in this synthesis. OH^- ion was reported to increase the electrostatic repulsion force between silver nanoprisms and to elevate the reducing ability of citrate.[28, 29] While in our system, OH^- ions were used to improve the uniformity of the silver seed nanoparticles and inhibit the generation of silver source to kinetically control the growth process. Motivated by the well-defined shape, large electric field enhancement (compared to truncated TSNPRs) was

Cite this: DOI: 10.1039/c0xx00000x

www.rsc.org/xxxxxx

ARTICLE TYPE

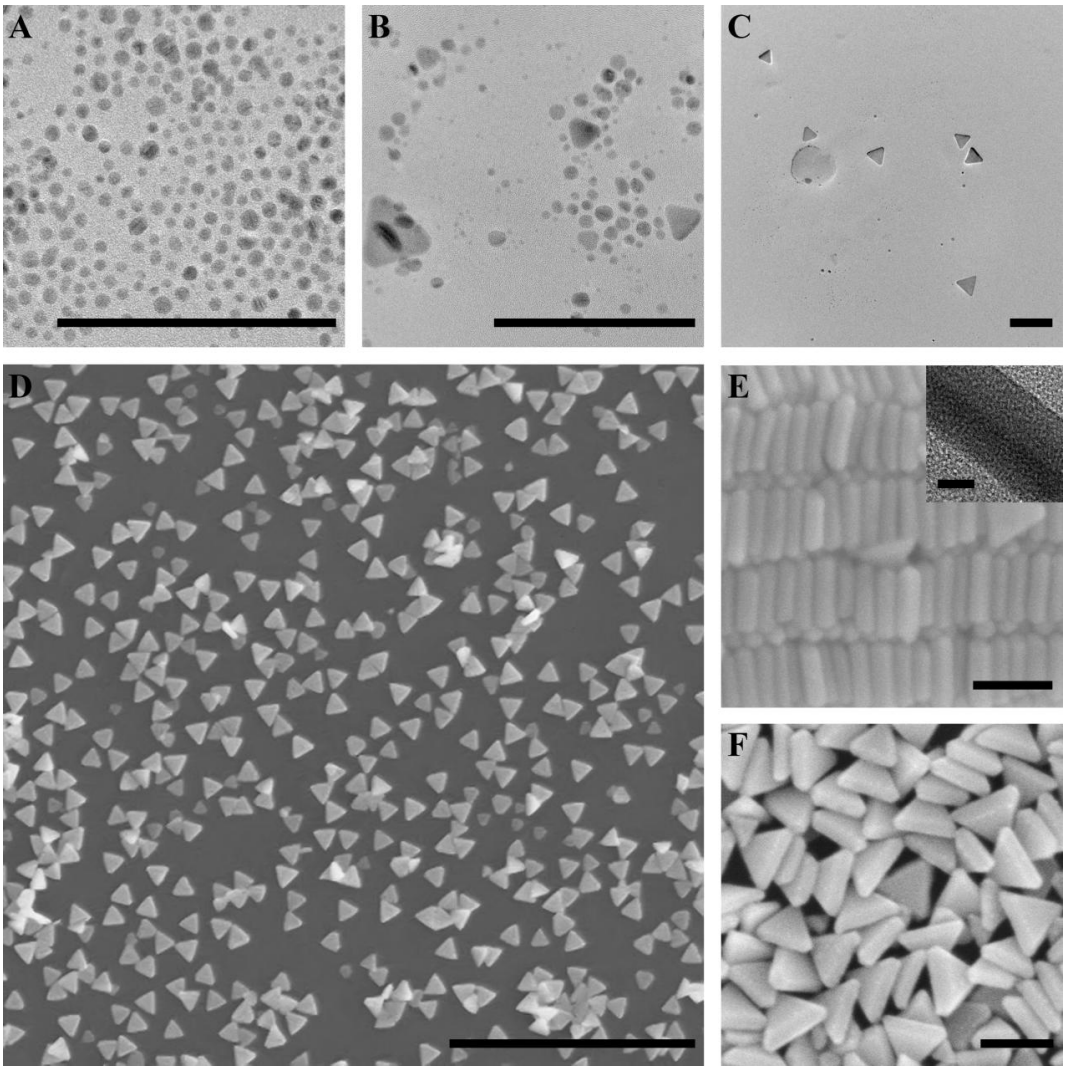

Figure 1. TEM images and SEM images of nanoparticles. Images of A, B, C, D corresponding the morphology changes of silver nanoparticles at different irradiation time: 0 min, 25 min, 35 min, 120min. Images of E, F representing the final morphology of silver nanoprisms in different scales and views. Inset picture of Figure E shows the TEM image of the thickness of TSNPRs. Scale bars: A~C, E~F are 100 nm, D is 1 μm. Scale bar of the inset picture in Figure E is 10 nm.

explored. Importantly, these monodisperse TSNPRs, as building blocks, enable us to form highly ordered and large-scale self-assembly structures consisting of six-tip based "hot spots", which display high enhancement (as high as 10^7) of SERS. Moreover, it was shown that these TSNPRs possess ultra-high local surface plasmon resonance sensitivity, which is among the highest level reported to date.

2. Experimental section

2.1 Materials

Silver nitrate (AgNO3, ≥99.8%), sodium hydroxide (NaOH, ≥98%), trisodium citrate (≥99%) were purchased from Beijing Chemical Works, sodium borohydride (NaBH4, ≥98%), 4-mercaptobenzoic acid (4-MBA, ≥90%), glycerol (≥99%) were purchased from Aldrich. Water was distilled and deionized using a Millipore Milli-Q Purification System, which has a resistivity of not less than 18.2 MΩ.

2.2 Synthesis of TSNPRs

24.25 ml deionized water, $AgNO_3$ (250 μL, 10 mM), and trisodium citrate (250 μL, 100 mM) were mixed under vigorously stirred at room temperature. To this mixture, 250 uL mixed aqueous solution ($NaBH_4$ (8 mM), NaOH (0.125M)) was injected via dropwise addition. The resulting silver seeds were instantly

Cite this: DOI: 10.1039/c0xx00000x

www.rsc.org/xxxxxx

ARTICLE TYPE

irradiated with a 70-W sodium lamp for 2 hours. Stirring was not stopped during the irradiation.

2.3 Preparation of self-assembled TSNPRs

15 ml solutions of TSNPRs were concentrated to 1 ml by centrifugation at 8500 rpm for 10 min. The resulted 1 ml of concentrated TSNPRs were further concentrated by centrifugation at 8500 rpm for 10 min. The final concentrated dispersion (ca. 20 μL) was deposited on silicon wafer, then, dried slowly to form the self-assembled structures.

2.4 SERS measurements

180 μL of purified nanoparticles (2 mL solutions, 8500 rpm for 10 min) and 20 μL of 4-MBA (0.5 mM) were mixed overnight. Then the samples were measured with QE 65 Pro spectrometer. Accumulation time was 1s for 500 mM 4-MBA solutions and substrates, 0.1 s for SERS of self-assembled samples, 10 s for SERS of good TSNPRs, 20 s for SERS of poor TSNPRs and power of laser was 250 mW. 500 mM aqueous solution of 4-MBA were prepared through adding NaOH (1 M) as reference samples. For self-assembled samples, 3 μL of 4-MBA (5 μM) were dropped on the silicon wafer with self-assembled structures for SERS measurements.

2.5 Refractive index sensitivity measurement

Refractive index of the surrounding medium of TSNPRs was changed by varying volume ratios of water-glycerol solutions. The volume percentage of glycerol changed from 10 % to 50 %. 1 mL TSNPRs were concentrated to 100 μL (8500 rpm for 10 min). Then 5μL concentrated TSNPRs redispersed into the water -glycerol solutions (1 mL). The LSPR peak position was plotted against of the refractive index. The refractive index sensitivity obtained through fitting the slope of the graph.

2.6 Instrumentation

A 70-W sodium lamp purchased from Osram China Lighting (emission spectra shown in Figure S1). Ultraviolet-visible (UV-VIS) absorption was recorded on a UV-3101PC UV–Vis–NIR scanning spectrophotometer (Shimadzu). The transmission electron microscopy (TEM) was performed on a Tecnai G2 F20 S-TWIN D573 electron microscope operated at 300 kV TEM. Scanning electron microscope (SEM) was performed on a field emission scanning electron microscopy (FESEM, Hitachi, S-4800). Ocean Optics QE 65 Pro spectrometer was used to record Raman spectra. InPhotonics 785 nm Raman fiber optic probe were used for excitation and data collection which combining 105 μm excitation fiber and 200 μm collection fiber, numerical aperture (NA) is 0.22. The light intensity of sodium lamp was measured by a photodiode power sensor (Thorlabs S120C).

3. Results and discussion

TSNPRs were synthesized based on plasmon-mediated method via converting spherical silver nanoparticles (Ag NPs) to triangular nanoprisms. The basic elements of plasmon-mediated method include light, citrate, oxygen, and small Ag NPs.[4] Oxygen could oxidize small Ag NPs to generate Ag^+ ions as silver source, and then light induces surface plasmon resonance

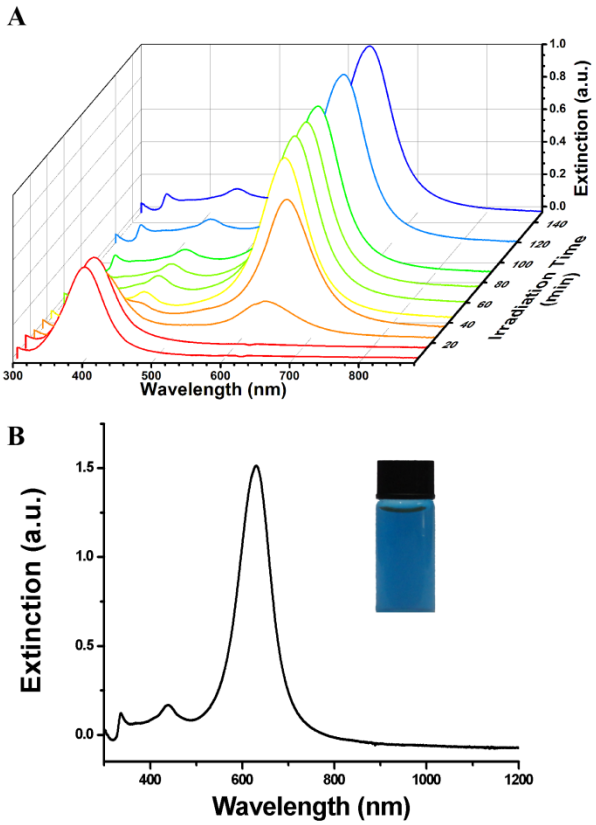

Figure 2. (A) UV-Vis spectra changes of reaction solutions obtained at different irradiation time when synthesizing TSNPRs; (B) UV-Vis-NIR spectra the final TSNPRs, the inset picture shows the final color of the solutions.

of Ag NPs to drive citrate reducing Ag^+ ions to silver atoms, resulting in the growth from Ag NPs to TSNPRs. In our reaction system, exciting SPR of Ag NPs is also required. In the absence of silver seeds, no reaction was observed in the mixture solutions of Ag^+ ions, citrates, OH^- ions with 8 hours light irradiating. (Figure S2).Without light irradiating or bubbling solution to remove oxygen, TSNPRs were failed to synthesize. When our system included all the basic elements for plasmon-mediated method, Ag NPs were gradually converted to TSNPRs. The initial spherical nanoparticles with an average diameter of 4.3 nm were prepared through chemical reduction method (Figure 1A, see Experimental Section for details). After irradiation of 25 minutes, small TSNPRs with edge length ranged from 11 to 18 nm appeared, whereas most of the particles remained spherical shape (Figure 1B). After 35 minutes of irradiation, more TSNPRs were formed and only a small portion of Ag NPs remained spherical shape (Figure 1C). The range of mean edge length of TSNPRs increased up to about 35-53 nm. Two hours later, nearly all nanoparticles were converted to TSNPRs (Figure 1D). The average length and thickness of TSNPRs was about 88 nm and 24

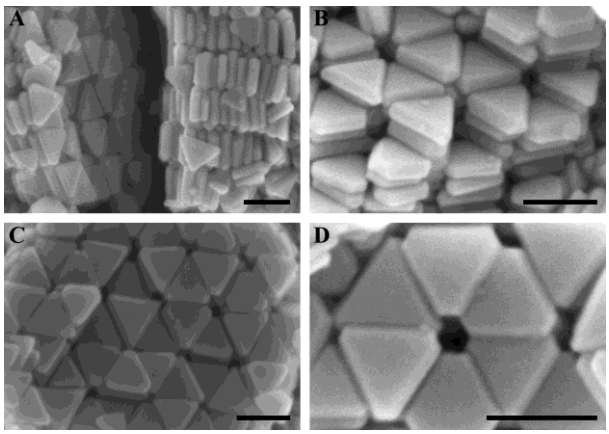

Figure 3. SEM images of self-assembly of silver nanoprisms in different views. All scale bars are 100 nm.

nm (Figure 1D~E), respectively. All these suggest that during the conversion process, TSNPRs were gradually grown up on the expense of the spherical Ag NPs. The final TSNPRs were nearly perfect triangular shape. Figure 1F shows that the edges of TSNPRs were a little rounded off.

This evolution process could also be confirmed by UV–Vis spectra (Figure 2A). The LSPR peak at ~395nm is characteristic for small spherical Ag NPs. This peak of Ag NPs was gradually decreased and finally disappeared implying that silver nanoparticles were continuously consumed. Ag NPs gradually disappeared, which arose from that they were dissolved by O_2 and then provided a source of Ag^+ thus could be re-deposited onto the other growing Ag NPs.[34, 35] The LSPR peaks centred at ~340 nm , ~440 nm and ~ 630 nm corresponded to the out-of-plane quadrupole, in-plane quadrupole and in-plane dipole plasmon resonance modes of TSNPRs.[22] The intensity of peak ~630 nm was increasing to the maximum during the reaction process implying that silver nanoprims were gradually formed. The final color of solutions was blue (Figure 2B). Except the absorption peaking at 630 nm, no absorption was observed in the range of 600-1100 nm (Figure 2B) indicating that no fusing of TSNPRs was happened.

The resulting TSNPRs show uniform shape (Figure 1D-F) and narrow size distribution (~83 nm) (Figure 2B). As a further proof of uniformity of these nanoparticles, we used these TSNPRs to perform self-assembly by simply evaporating concentrated nanoparticles dispersions on silicon wafer. Figure S3 shows that TSNPRs could be closely packed together, and self- assembled in micrometers scale, which verified the monodispersity of TSNPRs. The key step of self-assembly is to prepare monodisperse nanoparticles as building blocks. Actually, only uniform TSNPRs could be closely packed. From the breakage of columnar self-assembled structures (Figure 3A), it was obvious that silver nanoprisms packed closely with each other in the inner structures. It is known that six triangles can form a plane without any gaps. Thus these triangular nanoprisms could perfectly pack into a plane to form tight structures. These closed packing structures could be clearly seen from various angles (Figure 3B-D). Usually, two plasmonic metal nanoparticles approach each other, forming so-called "hot spots" which can largely enhance the electric field in the interparticle gaps.[36, 37] Recently, Dujardin *et al.* showedthat two triangular gold nanoprims coupled to each other (tip to tip)

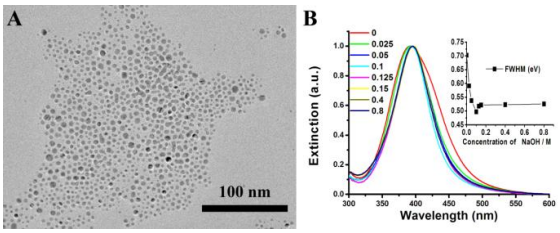

Figure 4. (A) TEM image of silver nanoparticles prepared in the absence of OH^-; (B) UV-Vis spectra of silver nanoparticles synthesized in different concentration of OH^-, inset shows changes of full width at half maximum (FWHM), the unit of Y axis is eV.

generated drastic couple field.[14] In our tight structures, there were six TSNPRs (especially six tips) closing to each other. This means there will be six huge electric fields couple to each other, which may display significant near-field effects.

We attributed the success of our synthesis to two main reasons. On the one hand, we introduced OH^- to elevate the monodispersity of silver seeds. OH^- ions have been reported to increase the electrostatic repulsion force between silver nanoprisms and elevate the reducing ability of citrate.[24, 25] In our reaction system, small Ag NPs (<5 nm) were prepared as seeds. Adding OH^- led to polydispersity decreased from 4.4±1.4 nm (Figure 4A) to 4.4±0.8 nm (Figure 1A). This could be further confirmed by the narrower size distribution of Ag NPs upon introducing OH^- (Figure 4B). It is known that small Ag NPs tend to aggregate to decrease surface potential. Figure 4A shows that without adding OH^- ions, Ag NPs appeared certain aggregation. Adding OH^- ions could increase the electrostatic repulsion between nanoparticles,[24] thus inhibit the fusion of Ag NPs, and improve the dispersity. Moreover, when the concentration of OH^- is more than 0.025 M (250 μL mixed aqueous solution with $NaBH_4$), FWHM of Ag NPs kept nearly the same (inset picture of Figure 4B).

On the other hand, more importantly, OH^- ions improved the stability of these small Ag NPs. The size of silver seeds affects the oxidation process, which limits the conversion time. To fulfill the conversion, the size of silver seeds is smaller than 10 nm.[23] Smaller silver nanoparticles are more susceptible to oxidation than larger nanoparticles due to their lower redox potentials.[34] In the early work by Mirkin *et al.*[22] ~8 nm sphere Ag nanoparticles were used as seeds, the conversion time was as long as 70 hours. Xia *et al.* [28] used 5.6±3.9 nm silver nanoparticles as seeds, and spent 40 hours to fulfill the conversion from silver nanoparticles to silver nanoprisms. Big Ag seeds usually result in long conversion time which is time-consuming and energy-consuming. More importantly, silver nanoprisms may be truncated during the long conversion process.[38] To circumvent these drawbacks, we have improved the oxidation process by introducing smaller ~4.3 nm sphere Ag nanoparticles as silver seeds to make silver seeds oxidize easier. However, these ~4.3 nm silver seeds were very instable. They will be oxidized at room temperature (Figure S3A). Without OH^- ions, the absorption peak decreased to 20 % (Figure S3A) within 45 minutes at room temperature (~25 ℃), indicating that ~80 % of small Ag NPs was oxidized to Ag^+. Fortunately, we introduced OH^- ions to make these ~4.3 nm silver seeds more

stable for reaction.

Oxidation of Ag NPs was evidently restrained by introducing OH^- ions by the shift of the absorption peak of Ag NPs in Figure S3. The absorption peak is sensitive to the concentration of Ag NPs, which could label the oxidation process of Ag NPs.[30, 34] Introducing more OH^- ions, the absorption peak intensity declined in a slower rate (Figure S3B-F), which indicated that oxidation rate became slower due to the suppression effect of OH^-. Actually, for synthesis of TSNPRs following plasmon-mediated method, the light irradiation resulted in gradual increase of the solution temperature (Figure S4). The rising temperature would accelerate the dissolving process of Ag NPs, which may make kinetic control growth deteriorate even further. Figure S3G shows that Ag NPs were quickly dissolved more than 90 % within 10 minutes when the solution temperature increased from 25 ℃ to 80 ℃. Fortunately, when introducing sufficient OH^- ions (such as 250 μL, 0.125 M OH^-), Ag NPs were stable when the solution temperature increased to 80 ℃ within 10 minutes and kept 80 ℃ for one hour (Figure S3H, S3I). Though light irradiation would accelerate the oxidation process of small Ag NPs due to the lifting of the temperature, OH^- ions would effectively inhibit this side effect.

The reasons why OH^- ions could make Ag NPs more stable are explained as follows. On the one hand, as it is known, Ag NPs were easily oxidized by O_2 due to the higher reduction potential of O_2 (E_0 (O_2/H_2O) = 1.23 V > E_0 (Ag^+/Ag) = 0.8 V).[39] On the one hand, reduction potential of O_2 could be decreased at high pH,[40] thus introducing OH^- ions could lower the oxidation ability of O_2 and inhibiting the oxidation of Ag NPs. On the other hand, OH^- ions, as the products of silver oxidation, also inhibit the oxidation reaction. The oxidation reaction of Ag NPs in water can be represented by equation (1)[41] or equation (2)[34]:

$$Ag_{(s)} + \frac{1}{2}O_{2(aq)} + 2H^+_{(aq)} \leftrightarrow Ag^+_{(aq)} + H_2\,O_{(l)} \quad (1)$$

$$Ag_{(s)} + \frac{1}{2}O_{2(aq)} + H_2\,O_{(l)} \leftrightarrow Ag^+_{(aq)} + 2OH^-_{(aq)} \quad (2)$$

In essence, these two equations are the same due to the ionization of water represented by following equation (3):

$$OH^-_{(aq)} + H^+_{(aq)} \leftrightarrow H_2\,O_{(l)} \quad (3)$$

Similar to previous report,[43] the release rate of Ag^+ ions with a little modification can be expressed as (details in supporting information):

$$\gamma_{Ag^+} = \frac{3}{4} \times 10^{-28}(\mathrm{mol/L})^4\left(\frac{8\pi k_B T}{m_A}\right)^{1/2} \rho^{-1} \exp\left(\frac{-E_a}{k_B T}\right)[Ag]r^{-1}[O_2]^{0.5}[OH^-]^{-2} \quad (4)$$

where γ_{Ag^+} represents the release rate of Ag^+ ions, $[O_2]$ and $[OH^-]$ are the molar concentration of oxygen and OH^-, respectively, [Ag] is the mass concentration, r is diameters of Ag NPs, m_A is the molar weight of silver, ρ is the density of silver, k_B is the Boltzmann constant, T is temperature and E_a is the activation energy. According equation (4), the release rate of Ag^+ ions is inversely proportional to the square of concentration of OH^-. Therefore, introducing OH^- ions could evenly inhibit the oxidation of Ag NPs in principle.

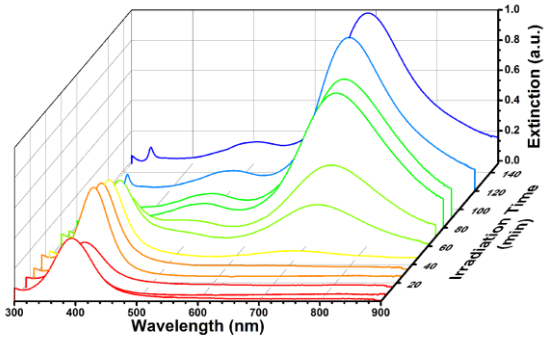

Figure 5. UV-Vis spectra changes of reaction solutions obtained at different irradiation time when the silver nanoprisms synthesized without adding OH^- ions.

Base on the observation of Figure S3, we could explain the phenomena in Figure 5. As it was mentioned before, the Ag NPs were instable. Heating effects resulting from irradiation (Figure S4) will accelerate the dissolution of Ag NPs to produce Ag^+ according equation (4) and Figure S3G. So these Ag NPs dissolved quickly, resulting in the decrease of the absorption peak of ~395 nm. Thus, Ag^+ ions might be reduced by unreacted $NaBH_4$ to produce Ag NPs again and the absorption ~395 nm recovered. This disappearing and recovering process of Ag NPs in Figure 5 indicates that Ag NPs were instable due to heating effects resulting from sodium lamp, and is unfavorable for kinetic control reactions. While introducing OH^- could stabilize Ag NPs, which resulted in the kinetically controlled growth for synthesizing uniform TSNPRs. The LSPR peak at ~395 nm gradually decreased and finally disappeared (Figure 2A) with irradiation time implied that Ag NPs were continuously consumed, rather than quickly dissolved and recovered process (Figure 5).

It should be noted that without adding OH^- ions, kinetic control growth of TSNPRs was also fulfilled to certain extent. Without adding OH^- ions, the initial absorption peak was at ~395 nm. After dissolving and recovering, absorption peak red-shifted to ~400 nm, indicating Ag NPs became bigger.[42] This bigger size was confirmed by TEM images (from initial 4.3 nm (Figure 4A) to 5.8 nm (Figure S5)). According to equation (4), Ag^+ ions release rate is inversely proportional to the radius of Ag NPs. This means bigger Ag NPs has slower generation rate of Ag^+ ions, which fulfilled kinetic control growth. Though big Ag NPs showed potential to make Ag NPs stable for fulfilling kinetic control growth, the diameters of nanoparticles were difficult to be controlled as a parameter for kinetically control growth. Moreover, bigger Ag NPs have higher redox potential and are difficult to be oxidized resulting in longer reaction time, TSNPRs may be truncated during the long conversion process.[38] Though small Ag NPs (<5 nm) were easier to be oxidized due to less conversion time, they were instable, were difficult to be controlled for growth. Introducing OH^- ions could stabilize small Ag NPs, and made these Ag NPs steadily convert to TSNPRs

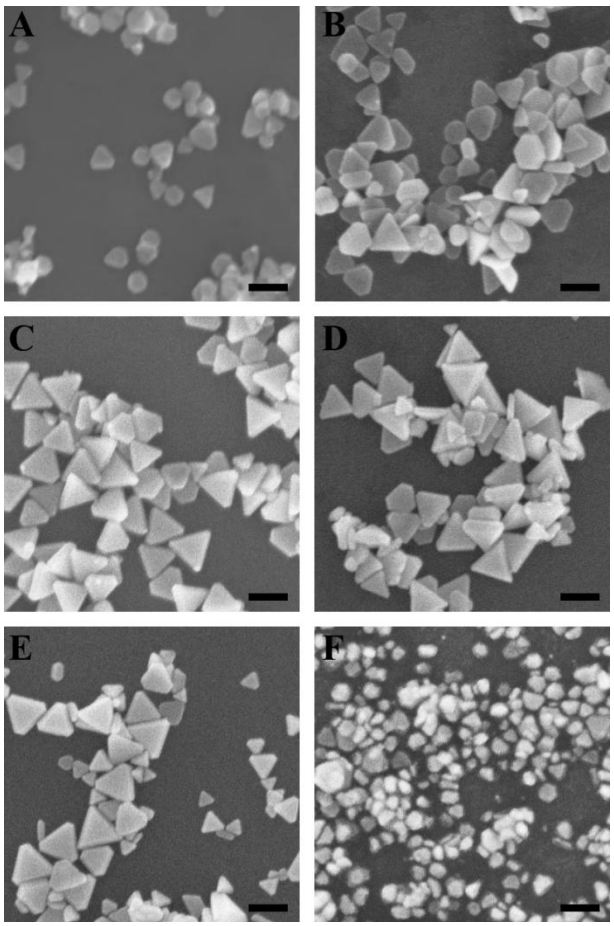

Figure 6. SEM images of silver nanoprisms synthesized in different addition concentration of OH^-: (A) 0 M; (B) 0.025 M; (C) 0.1 M; (D) 0.15 M; (E) 0.4M; (E) 0.8M. All scale bars are 100 nm.

(Figure 2A).In addition, adding more OH^- ions are found to be beneficial to synthesize high quality TSNPRs. As introduced before, OH^- ions make Ag NPs more uniform as seeds, which is favourable to synthesize monodisperse TSNPRs. When the concentration of OH^- ions went beyond 0.025 M, the uniformity of the silver seeds could not be further improved (Figure 4B), but TSNPRs became more uniform. The more OH^- ions added (from 0 to 0.125 M), the more uniform TSNPRs synthesized (Figure 6A-6C, Figure 1D). These results imply another key role of OH^- ions influencing the growth process.

Mirkin *et al*. demonstrated that plasmon-mediate reduction rate increased at high pH.[25] In their reaction system, solutions with silver seeds, $AgNO_3$, citrates, OH^- ions were irradiated with light. They used $AgNO_3$ as a source of Ag^+ rather than silver nanoparticles. Due to their solution having sufficient Ag^+ ions, the generation rate of silver atoms was determined by the reduction rate. At high pH, a fast reduction rate result in a fast reaction rate, generating high concentration of silver atoms, generating high concentration of silver atoms induces preferential deposition on (111) facets and leads to the formation of (100)-faceted right triangular bipyramids. At low pH such as 7, a slower reduction rate result in slower reaction rate, generating low concentration of silver atoms, induces silver atoms favouring deposition on (100) facets, triangular nanoprisms became the major morphology. Therefore, in their reaction system, low concentration of OH^- ions gives rise to slow reaction rate, which is favourable for synthesizing TSNPRs. High concentration of OH^- ions lead to a fast reaction rate, which is not favorable for synthesizing TSNPRs.

Different from Mirkin *et al.* [25] using $AgNO_3$ as a source of Ag^+, whereas in our case silver source only came from oxidation of small Ag NPs. After oxidation of Ag NPs to generate Ag^+ ions, citrate reduces these generated Ag^+ ions to silver atoms through plasmon-mediate method. Low concentration of silver atoms would deposit on favourable (100) facets, forming TSNPRs. Since the oxidation process happened before reduction process in our system, the rate of oxidation process to supply silver source is slow, the final reaction rate will be slow, irrespective of the rate of reducing rate. When the oxidation process is stopped, *i.e.* no Ag^+ ions produced, the overall reaction will be stopped. Therefore, the oxidation process dominants the reaction rate when the silver source is solely from the oxidation of Ag NPs. Based on this picture, the overall reaction rate was limited by the production of Ag^+ ions which was heavily depended on the amount of OH^- ions. The latter could inhibit the oxidation of Ag NPs to produce Ag^+ ions. As a result, the more OH^- ions are added, the severer the inhibiting effect of oxidizing Ag NPs, the slower the release rate of Ag^+ ions, the slower the production of silver atoms, which favours deposition of silver atoms onto favourable facets of Ag NPs (such as Ag (110) facet), and ends up with higher quality TSNPRs (Figure 6A-6C, Figure 1D).

We have also proved that the amount of OH^- has an up-limit for producing TSNPRs. TSNPRs became polydisperse and other irregular shapes appeared (Figure 6D-6F) when the concentration of OH^- was higher than 0.125 M in 250 μL addition solution. This might result from that too strong suppressing hindered the oxidation of Ag NPs, and then lowered the yield of TSNPRs. This too strong inhibition effect is confirmed by Figure S6A-C, which show the UV-Vis spectra of the solution during the synthesis process with concentration of OH^- higher than 0.125 M. The absorption around 400 nm decreased less and less when OH^- concentration was beyond 0.125 M in the 250 μL addition solution, which indicated that more and more Ag NPs could not be transformed into TSNPRs owing to the stronger suppress effects of higher concentration of OH^-. Meanwhile, the absorption around 630 nm became weaker when introducing more OH^-, indicating that the production yield of TSNPRs was lower. Though more OH^- means stronger inhibiting effect of Ag NPs for slower generating Ag^+ which is favourable for TSNPRs production, too much OH^- hinders the generation of Ag^+, until no Ag^+ generated anymore. The reaction even stopped after 30 minutes (Figure S6A-C). Due to too strong suppression, TSNPRs became more poly-dispersive with drastically low yield (Figure 6D-6F and S6D). The absorption ~500 nm may result from the smaller TSNPRs and irregular shapes (Figure 6D-6F). Besides the suppression effect of OH^-, too high concentration will cause a precipitation of AgOH and/or Ag_2O owing to the low Ksp of AgOH (1.52×10^{-8}),[43] which could also lower the production yield of TSNPRs.

Stirring shows also an important role in our synthesis. Some Ag NPs must be dissolved by oxygen to provide a source of

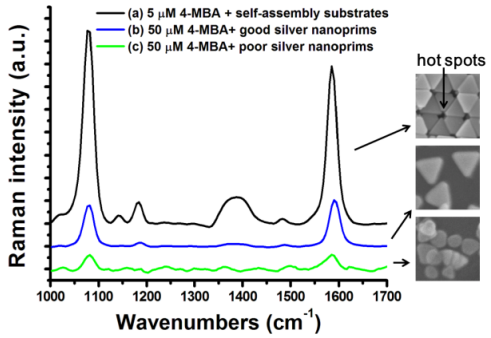

Figure 7. Raman spectrum of: (a) 5 μM 4-MBA with self-assembly structures of silver nanoprisms, accumulation time was 0.1 s; (b): 50 μM 4-MBA with good silver nanoprisms, accumulation time was 10 s; (c): 50 μM 4-MBA with poor silver nanoprisms, accumulation time was 20 s.

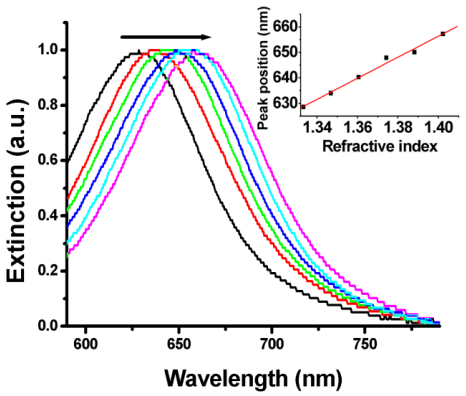

Figure 8. Extinction spectra of TSNPRs depersed in water-glycerol solutions of varying compositions. The inset picture shows the dependence of plamon peak shift on the refractive index of the water-glycerol mixture (0, 10, 20, 30, 40, and 50 vol % glycerol aqueous solutions), and the line is linear fit.

Ag^+.[34] On the one hand, during the growth process of TSNPRs, oxygen would be consumed in solution. On the other hand, during the growth process, temperature gradually increased (Figure S4) which would reduce the solubility of oxygen in water.[44] Driven by these two factors, dissolved oxygen in water became less and less. As oxygen was a necessity of our plasmon-mediated method, certain amount of oxygen needed to be kept in water.[37] Therefor, bubbling the solution with argon gas to remove oxygen, the yield decreased largely (Figure S7A). But when without stirring, we also got the decreased yield of TSNPRs (Figure S7B) similar to the condition of removing oxygen (Figure S7A). Stirring have been found to supply oxygen from air to water to keep the dissolved oxygen concentration for fermentation.[45] We infer that in our reaction system, without stirring, oxygen could not be supplied from air to water. Moreover adding OH^- ions could severely inhibit the oxidation of Ag NPs as we have discussed. Combining these two factors, therefore, yield of TSNPRs decreased largely (Figure S7B). But when without adding OH^-, even without stirring, the TSNPRs could also be prepared without lowering yield (Figure S7C). This may because that lack of the inhibition oxidation effects of OH^- ions, though oxygen in water decreased with reaction proceeded, the decreased oxygen in water was enough to oxidize Ag NPs. So when adding OH^- ions and without stirring, the content of oxygen in water is not sufficient to oxidize Ag NPs due to the inhibition effects OH^- ions. Therefore, stirring had to remain in our case during the irradiation process to supply enough oxygen for the oxidation of Ag NPs.

Light intensity also affects the oxidation of Ag NPs. When we lowered the light intensity from usually 126.41 mW/cm^2 to 33.30 mW/cm^2, Ag NPs could not be oxidized and silver nanoprisms could not be synthesized (Figure S8). When the solution was irradiated with power density of 33.30 mW/cm^2, the temperature of solution was only increased from 19 ^{o}C to 28 ^{o}C. One may expect that the low temperature may hamper the oxidation of Ag NPs due to low light intensity. To exclude this possibility, we irradiated the solution with power density of 33.30 mW/cm^2 and heated the solution to 80 ^{o}C at the same time, oxidation of Ag NPs was still not observed (Figure S9). This indicates that heating was not sufficient to oxidize Ag NPs, whereas light is also necessary in oxidation of Ag NPs. To further study it, weirradiated the solution with higher power density of 77.91 mW/cm^2, silver nanoparticles were not oxidized, either (Figure S10). Until the light intensity increased to 110.85 mW/cm^2, Ag NPs began to be oxidized (Figure S11). Photon etching effects in our system is interesting. As it is well known, noble metal nanoparticles have photothermal effects. Recently, Wei *et al.* have demonstrated that, under irradiation at 2.0 W/cm^2, SPR could induce surface temperature of nanostructures raised to above 230 ℃.[46] We infer photon etching effects in our reaction system may also arise from the SPR induced photothermal effects. This phenomenon is complex and further study in the future is needed.

We explored the SERS activities of TSNPRs using common Raman probe (4-MBA). To evaluate the enhancement, we calculated the SERS enhancement factors (EFs) following the formula,[47] EF =(I_{SERS} / I_{Raman})× (N_{Raman} / N_{SERS}), where I_{SERS} and I_{Raman} donate the SERS and Raman spectra, respectively, N_{Raman} is the number of molecules for normal Raman measurement, N_{SERS} is the number for SERS, respectively. Based on the intensities of the peak ~ 1091 cm^{-1}, the SERS EFs (details in supporting information) were estimated as 1.13 ×10^7, 3.12 ×10^4, 1.23 ×10^3 for self-assembly substrates of TSNPRs, good TSNPRs and poor TSNPRs(samples of Figure 5A) , respectively (Figure 7, Figure S12-13). Compared the EF of good and poor TSNPRs, well-defined TSNPRs have higher enhancement effect (25 times higher) of SERS than poor TSNPRs. Since the excitation of 785 nm was off-resonant in both cases, we attributed the higher enhancement of good TSNPRs to the fact that good nanoprisms have more well-defined tips than poor nanoprisms. These tips could generate stronger electric field to enhance Raman signal.[12] Meanwhile, we observed the EFs of self-assembly substrate as high as ~10^7 as shown in Figure 7, which came from the "hot spot" existing in the nanostructures, especially these six-tip based "hot spot", demonstrating that these plasmonic self-assembly structures amplified largely the electric field. However, we could

Sample	Peak λ (nm)	Δλ(nm)/ RIU	ΔE(eV)/ RIU	FOM
Single Silver Nanoprisms[13]	Pk1 : 631	205	0.57	2.2
	Pk2 : 635	183	0.51	2.6
	Pk3 : 631	196	0.55	3.3
Gold Nanotube[48]	650	225	-	-
Gold Nanorods[49]	653	195	-	2.6
Single Gold Nanopyramid[50]	600	174-199	-	1.2-2.2
Gold Nanobipyramid[49]	645-1096	150-540	-	1.7-4.5
Gold Nanodisk array[51]	696	226	-	-
Single Silver Nanocubes[52]	Pk1: 351	-	0.79	1.6
	Pk2: 444	-	0.69	5.4
Silver Nanoprisms[53]	687	402	-	3.87
Gold Nanorice[54]	1600	801	0.388	1.3
Silver Nanoprisms[55]	504-1093	188-1096	0.59 -1.2	1.8-4.3
This Work	629	413	1.24	4.59

Table 1. Comparison of LSPR sensitivities reported to date for various nanostructures from previous reports tested using similar refractive index methods.

not determine how many molecules are there in the plasmonic hot spots, resulting in estimating the EFs of self-assembly substrate only in a quantitative way.

In addition, TSNPRs with sharp tips showed ultrasensitive optical response to changes in the surrounding environment. Figure 8 shows the LSPR shift of TSNPRs when suspended in water-glycerol solutions with various volume ratios (0, 10, 20, 30, 40, and 50 vol % glycerol aqueous solutions). The refractive index of water-glycerol solutions could be calculated according to the Lorentz-Lorenz equation (Figure S14).[49] By fitting the slope of LSPR shift versus refractive index in Figure 8, the obtained LSPR sensitivity of TNPRs was as high as 413 nm RIU^{-1} (1.24 eV RIU^{-1}) with LSPR peak at 629 nm, which exceeds previously reports to our knowledge within the same LSPR bands ~630 nm (Table 1). Figure of merit (FOM) defined by Sherry *et al*. is a common used method to compare different plasmonic nanostructures,[13] which can be expressed as the ratio of linear refractive index sensitivity to LSPR full width at half maximum (FWHM). Based on this definition, FOM value of our TSNPRs was 4.59, which is among the highest level reported to date (Table 1). Utilization of this ultra-high LSPR sensitivity, these TSNPRs offer opportunities for the development of new generation chem/bio-sensors.

Conclusions

We have improved one step plasmon-mediated method to make it suitable to produce high quality TSNPRs with sole citrates capped. ~4.3 nm Ag NPs as silver seeds was significantly improved the uniformity and stability by introducing OH^- ions. Inhibition oxidation process by OH^- ions lowered the generation rates of silver source, resulting in kinetically control growth quality TSNPRS. Well-defined TSNPRs, display better SERS effects. By virtue of their monodispersity, six-tip based "hot spots" was, for the first time, obtained by self-assembling silver nanoprisms into close-packed structures. Especially their close-packed structures with six-tip based "hot spots" the enhancement as high as $10^7$was reached. Moreover, these TSNPRs displayed ultra-high LSPR sensitivity (413 nm RIU^{-1} or 1.24 eV RIU^{-1}, FOM=4.59) at ~630 nm.

Acknowledgements

This work was financially supported by NSF of China (61071048, 11374297, 51372096), Joint research program between CAS of China and KNAW of the Netherlands, the IOP program of the Netherlands, and John van Geuns foundation. Many thanks to Prof. Xu Weiqing and Dr. Tang Bin (University of Jilin) for their help during this work.

Notes and references

a State Key Laboratory of Luminescence and Applications, Changchun Institute of Optics, Fine Mechanics and Physics, Chinese Academy of Sciences, Changchun 130033, China.
b Graduate University of the Chinese Academy of Sciences, Beijing 100049, China.
c Department of Basic Medicine, Gerontology Department of First Bethune Hospital, University of Jilin, Changchun 130021, China.
d Van't Hoff Institute for Molecular Sciences, University of Amsterdam, Science Park 904, 1098 XH Amsterdam, The Netherlands.
†These authors contributed equally to this work.
* *Corresponding author:*
E-mail: xgkong14@ciomp.ac.cn; h.zhang@uva.nl
†Electronic Supplementary Information (ESI) available:. See DOI: 10.1039/b000000x/

1. C. H. Chou and F. C. Chen, *Nanoscale*, 2014, **6**, 8444-8458.
2. M. Rycenga, C. M. Cobley, J. Zeng, W. Li, C. H. Moran, Q. Zhang, D. Qin and Y. Xia, *Chem. Rev.* , 2011, **111**, 3669-3712.
3. S. Zeng, D. Baillargeat, H. P. Ho and K. T. Yong, *Chem. Soc. Rev.* , 2014, **43**, 3426-3452.
4. M. R. Langille, M. L. Personick and C. A. Mirkin, *Angew. Chem. Int. Ed.* , 2013, **52**, 13910-13940.
5. J. E. Millstone, S. J. Hurst, G. S. Métraux, J. I. Cutler and C. A. Mirkin, *Small*, 2009, **5**, 646-664.
6. A. P. Kulkarni, K. M. Noone, K. Munechika, S. R. Guyer and D. S. Ginger, *Nano Lett.* , 2010, **10**, 1501-1505.
7. K. Yao, M. Salvador, C. C. Chueh, X. K. Xin, Y. X. Xu, D. W. deQuilettes, T. Hu, Y. Chen, D. S. Ginger and A. K. Y. Jen, *Adv. Energy Mater.*, 2014, **4**.
8. S.H. Ciou, Y. W. Cao, H. C. Huang, D. Y. Su and C. L. Huang, *J. Phys. Chem. C*, 2009, **113**, 9520-9525.
9. L. Xu, Z. Luo, Z. Fan, X. Zhang, C. Tan, H. Li, H. Zhang and C. Xue, *Nanoscale*, 2014, **6**, 11738-11743.
10. S. C. Boca, M. Potara, A. M. Gabudean, A. Juhem, P. L. Baldeck and S. Astilean, *Cancer Lett.*, 2011, **311**, 131-140.
11. C. Gao, Z. Lu, Y. Liu, Q. Zhang, M. Chi, Q. Cheng and Y. Yin, *Angew. Chem. Int. Ed.* , 2012, **51**, 5629-5633.
12. K. L. Kelly, E. Coronado, L. L. Zhao and G. C. Schatz, *J. Phys. Chem. B*, 2003, **107**, 668-677.
13. L. J. Sherry, R. Jin, C. A. Mirkin, G. C. Schatz and R. P. Van

Duyne, *Nano Lett.* , 2006, **6**, 2060-2065.
14. S. Viarbitskaya, A. Teulle, R. Marty, J. Sharma, C. Girard, A. Arbouet and E. Dujardin, *Nat. Mater.* , 2013, **12**, 426-432.
15. D. A. Rosen and A. R. Tao, *ACS Appl. Mat. Interfaces* 2014, **6**, 4134-4142.
16. K. M. Mayer and J. H. Hafner, *Chem. Rev.* , 2011, **111**, 3828-3857.
17. E. Martinsson, M. M. Shahjamali, K. Enander, F. Boey, C. Xue, D. Aili and B. Liedberg, *J. Phys. Chem. C*, 2013, **117**, 23148-23154.
18. X. Yang, Y. Yu and Z. Gao, *ACS nano*, 2014, **8**, 4902-4907.
19. B. Malile and J. I. Chen, *J. Am. Chem. Soc.* , 2013, **135**, 16042-16045.
20. Y. Xia, J. Ye, K. Tan, J. Wang and G. Yang, *Anal. Chem.* , 2013, **85**, 6241-6247.
21. L. Chen, X. Fu, W. Lu and L. Chen, *ACS Appl. Mat. Interfaces* 2012, **5**, 284-290.
22. R. Jin, Y. Cao, C. A. Mirkin, K. Kelly, G. C. Schatz and J. Zheng, *Science*, 2001, **294**, 1901-1903.
23. R. Jin, Y. C. Cao, E. Hao, G. S. Métraux, G. C. Schatz and C. A. Mirkin, *Nature*, 2003, **425**, 487-490.
24. C. Xue and C. A. Mirkin, *Angew. Chem. Int. Ed.* , 2007, **119**, 2082-2084.
25. J. Zhang, M. R. Langille and C. A. Mirkin, *J. Am. Chem. Soc.* , 2010, **132**, 12502-12510.
26. M. Maillard, P. Huang and L. Brus, *Nano Lett.* , 2003, **3**, 1611-1615.
27. H. Jia, W. Xu, J. An, D. Li and B. Zhao, *Spectrochim. Acta, Part A* 2006, **64**, 956-960.
28. Y. Sun and Y. Xia, *Adv. Mater.* , 2003, **15**, 695-699.
29. G. S. Métraux and C. A. Mirkin, *Adv. Mater.* , 2005, **17**, 412-415.
30. Q. Zhang, N. Li, J. Goebl, Z. Lu and Y. Yin, *J. Am. Chem. Soc.* , 2011, **133**, 18931-18939.
31. D. Aherne, D. M. Ledwith, M. Gara and J. M. Kelly, *Adv. Funct. Mater.* , 2008, **18**, 2005-2016.
32. Z. Niu and Y. Li, *Chem. Mater.* , 2013, **26**, 72-83.
33. N. Cathcart and V. Kitaev, *ACS nano*, 2011, **5**, 7411-7425.
34. C. Xue, G. S. Métraux, J. E. Millstone and C. A. Mirkin, *J. Am. Chem. Soc.* , 2008, **130**, 8337-8344.
35. X. Wu, P. L. Redmond, H. Liu, Y. Chen, M. Steigerwald and L. Brus, *J. Am. Chem. Soc.* , 2008, **130**, 9500-9506.
36. A. Klinkova, R. M. Choueiri and E. Kumacheva, *Chem. Soc. Rev.* , 2014, **43**, 3976-3991.
37. Q. Sun, K. Ueno, H. Yu, A. Kubo, Y. Matsuo and H. Misawa, *Light: Sci. Appl.*, 2013, **2**, e118.
38. J. An, B. Tang, X. Ning, J. Zhou, S. Xu, B. Zhao, W. Xu, C. Corredor and J. R. Lombardi, *J. Phys. Chem. C*, 2007, **111**, 18055-18059.
39. E. C. Cho, C. M. Cobley, M. Rycenga and Y. Xia, *J. Mater. Chem.* , 2009, **19**, 6317-6320.
40. M. Chuan, G. Shu and J. Liu, *Water, Air, and Soil Pollution*, 1996, **90**, 543-556.
41. W. Zhang, Y. Yao, N. Sullivan and Y. Chen, *Environ. Sci. Technol*., 2011, **45**, 4422-4428.
42. X. Fan, W. Zheng and D. J. Singh, *Light: Sci. Appl.*, 2014, **3**, e179.
43. D. R. Lide, *CRC handbook of chemistry and physics*, CRC press, 2004.
44. *Standard methods for the examination of water and wastewater*, 20th ed. published jointly by the American Public Health Association, American Water Works Association, and Water Environment Federation ,1998.
45. E. Parente, M. Crudele, M. Aquino and F. Clementi, *J. Ind. Microbiol. Biotechnol.* , 1998, **20**, 171-176.
46. J. Qiu, Y. C. Wu, Y. C. Wang, M. H. Engelhard, L. McElwee-White and W. D. Wei, *J. Am. Chem. Soc.* , 2012, **135**, 38-41.
47. E. Le Ru, E. Blackie, M. Meyer and P. G. Etchegoin, *J. Phys. Chem. C*, 2007, **111**, 13794-13803.
48. J. McPhillips, A. Murphy, M. P. Jonsson, W. R. Hendren, R. Atkinson, F. Ho□o□k, A. V. Zayats and R. J. Pollard, *ACS nano*, 2010, **4**, 2210-2216.
49. H. Chen, X. Kou, Z. Yang, W. Ni and J. Wang, *Langmuir*, 2008, **24**, 5233-5237.
50. J. Lee, W. Hasan and T. W. Odom, *J. Phys. Chem. C*, 2009, **113**, 2205-2207.
51. M. Sanders, Y. Lin, J. Wei, T. Bono and R. G. Lindquist, *Biosens. Bioelectron.* , 2014, **61**, 95-101.
52. L. J. Sherry, S.-H. Chang, G. C. Schatz, R. P. Van Duyne, B. J. Wiley and Y. Xia, *Nano Lett.* , 2005, **5**, 2034-2038.
53. M. M. Shahjamali, M. Salvador, M. Bosman, D. S. Ginger and C. Xue, *J. Phys. Chem. C*, 2014, **118**, 12459-12468.
54. H. Wang, D. W. Brandl, F. Le, P. Nordlander and N. J. Halas, *Nano Lett.* , 2006, **6**, 827-832.
55. D. E. Charles, D. Aherne, M. Gara, D. M. Ledwith, Y. K. Gun'ko, J. M. Kelly, W. J. Blau and M. E. Brennan-Fournet, *ACS nano*, 2009, **4**, 55-64.